Available online at www.sciencedirect.com
SCIENCE DIRECT
Vision Research 46 (2006) 2703–2720
Vision Research
www.elsevier.com/locate/visres

Contribution of lateral interactions in V1 to organization of response properties

J.J. Wright [a,b,*], D.M. Alexander [c], P.D. Bourke [d]

[a] Liggins Institute, University of Auckland, Auckland, New Zealand
[b] Brain Dynamics Centre, University of Sydney, Sydney, Australia
[c] Faculty of Information Technology, University of Technology, Sydney, Australia
[d] Centre for Astrophysics and Supercomputing, Swinburne University, Melbourne, Australia

Received 15 August 2005; received in revised form 4 December 2005

Abstract

We propose a model of self-organization of synaptic connections in V1, emphasizing lateral interactions. Subject to Hebbian learning with decay, evolution of synaptic strengths proceeds to a stable state in which all synapses are either saturated, or have minimum pre/post-synaptic coincidence. The most stable configuration gives rise to anatomically realistic "local maps", each of macro-columnar size, and each organized as Mobius projections of retinotopic space. A tiling of V1, constructed of approximately mirror-image reflections of each local map by its neighbors is formed, accounting for orientation-preference singularities, linear zones, and saddle points—with each map linked by connections between sites of common orientation preference. Ocular dominance columns are partly explained as a special case of the same process. The occurrence of direction preference fractures always in odd numbers around singularities is a specific feature explained by the Mobius configuration of the local map. Effects of stimulus velocity, orientation relative to direction of motion, and extension, upon orientation preference, which are not accounted for by spatial filtering, are explained by interactions between the classic receptive field and global V1.

Keywords: Primary visual cortex; Lateral interactions; Neural networks; Orientation; Neuroanatomy

1. Introduction

This paper addresses three areas of controversy in visual neuroscience. First, the role of lateral cortical connections in visual processing within visual cortex (V1); secondly, the relationship of Hebbian learning to dimension-reduction explanations of V1 architecture; thirdly, the role played by synchronous oscillation. Considering these in order:

Stimulation of a small locale in the visual field (the receptive field (RF)) brings forth a response in the 40–60 ms lag range, in a small cortical locale corresponding to the field of projection of the RF to V1 (Angelucci & Bullier, 2003; Li, Their, & Wehrhahn, 2000), and V1 has been shown to process information from correspondingly small locales of the visual field (De Valois, De Valois, & Yund, 1979; Movshon, Thompson, & Tolhurst, 1978; Schiller, Finlay, & Volman, 1976). The classical view of feed-forward processes in the direct visual pathway is that surround inhibitory fields produce spatial filtering of input signals, enhancing movement, lines and edges, and giving rise to orientation preference (OP). Several groups have modified this view. Ringach, Hawken, and Shapley (1997) showed that intracortical feedback appears to change OP on a dynamic basis. Chavane et al. (2000) drew attention to the interaction of receptive field responses and activity in the visual cortical surround, and Series, Georges, Lorenceau, and Fregnac (2002) have produced a neural network model of lateral interactions in V1 to account for interactions of stimulus orientation and apparent speed.

* Corresponding author. Fax: +64 9 4820 927.
E-mail addresses: jj.w@xtra.co.nz (J.J. Wright), dalex@it.uts.edu.au (D.M. Alexander), pdb@swin.edu.au (P.D. Bourke).

0042-6989/$ - see front matter © 2006 Elsevier Ltd. All rights reserved.
doi:10.1016/j.visres.2006.02.017

The majority of synapses on V1 neurons are formed by lateral connections arising from neurons with somata distributed over a wide range of cortical separations (Braitenberg & Schuz, 1998) and modeling supports the propagation of signals in a wave-like manner via polysynaptic pathways (e.g., Jirsa & Haken, 1996; Robinson, Rennie, & Wright, 1998). When V1 is stimulated by direct pathway projections, some of the evoked responses occur at greater delays than 40–60 ms, and at greater distances than the classical receptive field (Slovin, Arieli, Hildesheim, & Grinvald, 2002), consistent with lateral spread of information via polysynaptic routes.

A number of recent papers have related the electrophysiological responses of neurons to the spatial ranges of various connection systems (Angelucci & Bullier, 2003; Angelucci et al., 2002; Levitt & Lund, 2002). A recent critical review (Alexander & Wright, 2006) shows the maximum scale of excitatory modulation in V1 may be the size of V1 itself. There is clear evidence of the importance of lateral, as well as descending, influences as major controls of activity throughout the visual pathway (e.g., Angelucci et al., 2002; Lamme, Super, & Spekreijse, 1998; Lee, 2002; Stein & Sarnthein, 2000). In some situations a neuron can be driven solely by extra-RF stimulation: foveal V1 cells can be driven by a bar whose entire extent within the RF is obscured by a patch that is in the foreground relative to the bar (Sugita, 1999); long moving bars can still fire V1 neurons when artificial scotomas cover the RF (Fiorani, Rosa, Gattass, & Rocha-Miranda, 1992); 26% of V1 neurons will respond to the illusory contours of Kanizsa squares (Lee, 2002); over half of V1 neurons can be driven by moving gratings presented within an annulus (Cavanaugh, Bair, & Movshon, 2002); a textured field with a large hole over the RF fires 93% of V1 neurons tested (Rossi, Desimone, & Ungerleider, 2001).

Mathematical models of connections in V1 began with the "ice-cube" model (Hubel & Wiesel, 1968, 1977). This classic model has subsequently proved to have considerable limitations (Bressloff, 2002; Bressloff & Cowan, 2002). Explanatory models fall generally into two categories.

The first category includes models depending upon neural network principles, which originate from the work of von der Marlsburg (e.g., Bressloff, 2002; Bressloff & Cowan, 2002; Goodhill, 1993; Grossberg & Williamson, 2001; Linsker, 1986; Miller, Keller, & Stryker, 1989; Obermayer, Ritter, & Schulten, 1990; von der Marlsburg, 1973; Tanaka, 1989), showing that a variety of realistic spatial ordering of response properties emerges in two-dimensional arrays of neurons under Hebbian learning, with "Mexican Hat" local inhibitory surround architectures.

Models of the second category give an account of the same response organization in terms of dimension reduction (Durbin & Mitchison, 1990; Durbin & Willshaw, 1987; Kohonen, 1982; Mitchison & Durbin, 1986). Here, the higher dimensional complexity of information in the afferents is reduced to the two-dimensional cortical surface. Dimension reduction is achieved by a mapping endeavoring to satisfy goals of continuity and completeness—that is, the need to maintain local smoothness of response properties within the cortical sheet, and the need to ensure the sheet includes a compact, representative selection of points in stimulus space. Dimension-reduction mapping solutions yield results similar to the neural network models, but the interrelationship of the Hebbian and dimension-reduction accounts is unclear.

Both these classes of models encounter difficulties with some recent experimental findings—notably the sensitivity of OP to velocity, orientation relative to direction of motion, and extension, of moving textures (Basole, White, & Fitzpatrick, 2003).

At both long and short ranges, synchronous oscillation can be induced by concurrent stimulation of cortical sites (Gray, Engel, Konig, & Singer, 1992; Gray, Konig, Engel, & Singer, 1989; Singer & Gray, 1995). Consistent with experimental observations, theoretical modeling of synchrony (Chapman, Bourke, & Wright, 2002; Robinson et al., 1998; Wright, 1997; Wright, Bourke, & Chapman, 2000) shows that synchrony is a broadband phenomenon not restricted to the gamma range, is induced over bi-directional couplings, and develops in response to changes in stimuli after a lag comparable to the axonal delay between the sites. Synchrony offers a mechanism for the co-ordination of learning under Hebbian synaptic rules. Its relevance to the maximization of information stored in connections evolving under Hebbian learning has been demonstrated (Kay & Phillips, 1997; Phillips & Singer, 1997) but it is not known how this "coherent infomax" principle might become manifest in real neural organization.

We have earlier suggested (Alexander, Bourke, Sheridan, Konstandatos, & Wright, 1998, 2004) that the organization of OP arises from a tiling of the surface of V1 with local synaptic maps, each representing activity in the global map—that is, the extended surface of V1 – and having a singularity within each local map corresponding to the position of the local map within the global map. In this paper, we justify the earlier hypothesis by a theoretical treatment of the development of synaptic connections consequent to lateral interactions. We will show that continuity and completeness arises in local maps as a consequence of Hebbian learning with decay, mediated by fields of synchronous oscillation, and that the most stable synaptic configuration requires that the local map has a form analogous to a Mobius strip representation of the global map.

2. Theory

2.1. Mathematical conventions

X_j, Y_k; elements of the complex planes $\{X\},\{Y\}$
$Y_j \rightarrow X_k$; one to one map
$Y_j \Rightarrow X_k$; N to one map
Scalar distances, e.g., $|X_j - X_k|$ may be rendered as $|j - k|$ in context.

$A \propto B$ indicates a monotonic relation, rather than linear proportionality.

2.2. Simplified two-disk model

2.2.1. Configuration

An abstract system (see Fig. 1) which we will later apply to V1 in several modified forms, is comprised of two disks, respectively situated in two planes, $\{X\}$ and $\{Y\}$. The disks are two-dimensional continuum representations of the cortical surface, with positions within each disk given by complex numbers with ordered subscripts $1,2,\ldots,j,\ldots,k,\ldots,l,\ldots,n$. No explicit size constraint is required in the abstract representation. The two disks may be taken to represent areas each the size of macrocolumns, or one disk may be of macrocolumnar size, while the other may be as large as the entire extent of V1.

Symmetric bi-directional axo-synaptic couplings form uniform all-to-all connections between planes, and bi-directional all-to-all connections with synaptic density decreasing as a function of distance within each plane. That is, where σ indicates synaptic density; $\sigma(X_jY_k) = \text{constant}$, and $\sigma(X_jX_k) \propto |X_j - X_k|^{-1}$.

The general decline of the density of synapses generated by cortical pyramidal cells as a function of distance from the soma (e.g., Braitenberg & Schuz, 1998) is a crucial property upon which this model depends, because of the relation of coupling density to the magnitude of synchronous oscillation, as described in the next section. The uniform coupling density between planes is an initial simplification, which will be amended in application to real anatomical systems, in accord with Section 2.4.

Between disks, all connections are excitatory. The population of neurons within each disk is of mixed inhibitory and excitatory cells, and within each disk couplings via excitatory and inhibitory synapses create "Mexican Hat" surrounds.

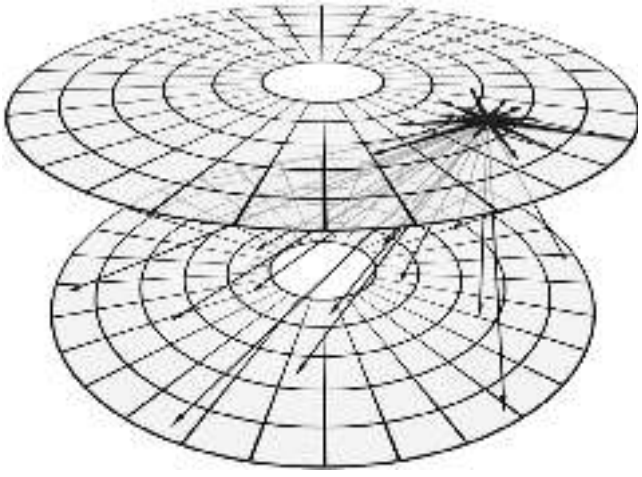

Fig. 1. Connections within and between continuum representations of cortical tissue. Top disk: black arrows show efferent connections from a representative point. The density of connection to other points declines with distance of separation. Lower disk: efferent connections from the representative point in the top disk terminate with uniform density.

2.2.2. Neural wave dynamics and synchrony

Theoretical work (Chapman et al., 2002; Freeman, 1975; Haken, 1996; Jirsa & Haken, 1996; Rennie, Wright, & Robinson, 2000; Robinson et al., 1998, 2003; Wright, 1997; Wright et al., 2000, 2003) (See Appendix A) enables neurons within each disk to be considered as a polysynaptic medium for the propagation of electrocortical waves, and to act as a medium for synchronous oscillation. Explicit use of these dynamic models is not required for the simulations and results that follow, but their account of synchronous oscillation (Chapman et al., 2002; Robinson et al., 1998; Wright, 1997) provides a mechanism for the co-ordination of synaptic modification in the present model.

Each disk is driven by externally imposed or internally generated synapto-dendritic activity approximating spatio-temporal white, or brown, noise. Mean pulse rates, $\overline{Q}_{e,i}$, are spatially uniform. Synchronous oscillation develops between reciprocally connected neurons. The mean and standard deviation of pulse trains and dendritic potentials between any two points is proportional to the sum (with appropriate sign and weight) of the densities of excitatory and inhibitory connections between the points, modified by gain factors, H_s, attributable to Hebbian modification of excitatory synapses.

Where R is a measure of synchrony (which may be measured by either spike co-incidence rate, or local field potential covariance), then between disks

$$R(X_jY_k) \propto \sigma(X_jY_k) \times \overline{H}_s(X_jY_k) \tag{1}$$

and within planes

$$R(X_jX_k) \propto [\sigma_e(X_jX_k) \times \overline{H}_s(X_jX_k) - \sigma_i(X_jX_k)]. \tag{2}$$

2.2.3. Learning rule

$R(X_jY_k)$ and $R(X_jX_k)$ in Eqs. (1,2) are measures that are directly proportional to the aggregate of the *pre/post-synaptic coincidence*, $r_{Q\varphi}$, at individual synapses connecting X_jY_k, X_jX_k, over short epochs, $n\Delta t$. Synchronous oscillation acts to co-ordinate synaptic gain modification, over bi-directional couplings, according to the following learning rule. Where pre/post-synaptic coincidence is defined by

$$r_{Q\varphi} = \frac{Q_{\max}}{n} \sum_t Q_e(t) \times \varphi_e(t) \quad t = t_0, \ldots, n\Delta t,$$
$$Q_e(t) \in \{0,1\}; \quad \varphi_e(t) \in \{0,1\} \tag{3}$$

where $Q_{\max}$ is the maximum action potential firing rate of neurons. In approximately steady-state conditions the mean post-synaptic pulse rate, $\overline{Q}_e$, is constant, equal to the pre-synaptic pulse rate, or afferent pulse density, $\bar{\varphi}_e$, and $Q_{\max} \gg \overline{Q}_e$.

Synaptic gain increases to saturation with high pre- and post-synaptic coincidence of depolarization, but decays if pre- and post-synaptic depolarization no longer coincide,

thus approximating rules of the "floating hook" type (Artola, Brocher, & Singer, 1990; Bienenstock, Cooper, & Monro, 1982; Hancock, Smith, & Phillips, 1991; Kay & Phillips, 1997). The steady-state Hebbian gain factor is

$$H_s = H_{\max}\exp[-\lambda/r_{Q\varphi}], \quad \lambda + ve, \tag{4}$$

where λ is a suitable constant.

The rise and fall of synaptic gain in response to a brief period of high pre/post-synaptic coincidence is described by the normalized impulse response function

$$H(t) = H_s(t-\tau) \otimes \frac{(\beta-\alpha)}{\alpha\beta}(\exp[-\beta\tau] - \exp[-\alpha\tau]), \tag{5}$$

where α and β are rise and fall time constants. This simple time–response can incorporate different mechanisms and rates of synaptic consolidation (and thus long and short-term memory) by defining a set of λ, α, and β applicable at different time-scales.

2.3. Conditions of synaptic stability in the two-disk model

2.3.1. Stability at individual synapses

Since pre- and post-synaptic firing rates approximate Poisson processes, the variance, $\varsigma^2(r_{Q\varphi}, \tau)$, of pre/post-synaptic coincidence measured during short epochs, τ, is proportional to the mean value, $\bar{r}_{Q\varphi}$, over a set of epochs., i.e.,

$$\varsigma^2(r_{Q\varphi}, \tau) \propto \bar{r}_{Q\varphi}. \tag{6}$$

Differentiating the steady-state synaptic gain (Eq. (4)) gives

$$\left.\frac{dH_s}{dr_{Q\varphi}}\right|_{\bar{r}_{Q\varphi}} = H_{\max}\frac{\lambda}{\bar{r}^2_{Q\varphi}}\exp[-\lambda/\bar{r}_{Q\varphi}]. \tag{7}$$

Therefore $S(H_s, \tau)$, the RMS deviation of synaptic gain as a function of $\bar{r}_{Q\varphi}$, is given by

$$\begin{aligned} S &= \left.\frac{dH_s}{dr_{Q\varphi}}\right|_{\bar{r}_{Q\varphi}} \times \varsigma(r_{Q\varphi}, \tau) \\ &= H_{\max}\frac{\lambda}{\bar{r}^2_{Q\varphi}}\exp[-\lambda/\bar{r}_{Q\varphi}] \times \sqrt{\kappa\bar{r}_{Q\varphi}}, \end{aligned} \tag{8}$$

where κ is a constant of proportionality, so

$$\frac{dS}{d\bar{r}_{Q\varphi}} = H_{\max}\lambda\sqrt{\kappa}\exp[-\lambda/\bar{r}_{Q\varphi}](\lambda\bar{r}^{-7/2}_{Q\varphi} - \tfrac{3}{2}\bar{r}^{-5/2}_{Q\varphi}). \tag{9}$$

From Eq. (8); since λ, κ, $H_{\max}$ are all +ve, then

$$\begin{aligned} &\text{if } \bar{r}_{Q\varphi} = 0 \text{ then } S = 0; \text{if } \bar{r}_{Q\varphi} = \infty \text{ then } S = 0; \\ &\text{if } 0 < \bar{r}_{Q\varphi} < \infty \text{ then } S + \text{ve}. \end{aligned} \tag{10.1}$$

From Eq. (9);

$$\text{setting}\frac{dS}{d\bar{r}_{Q\varphi}} = 0, \text{solutions are } \bar{r}_{Q\varphi} = 0, \infty, 2\lambda/3. \tag{10.2}$$

That is, $S(\bar{r}_{Q\varphi})$ has a single maximum at $\bar{r}_{Q\varphi} = 2\lambda/3$, and zero minima at $\bar{r}_{Q\varphi} = 0, \infty$, and therefore stable states of the synapse can occur only at either maximum saturation or zero saturation. We will subsequently refer to maximally saturated synapses as *saturated* and zero-saturated synapses as *sensitive*. (The latter term arises from the maximum slope of Eq. (4) which occurs at $r_{Q\varphi} = 0$, and the term is intended to emphasize that the zero-saturated synapse retains the capacity for relatively rapid and flexible change of state.)

2.3.2. Population synaptic stability

The time-decay of individual synaptic gains (Eq. (5)) favors evolution in the population toward global stability, analogous to the operation of the Metropolis algorithm in related thermodynamic systems (Kirkpatrick, Gelatt, & Vecchi, 1983). We will not prove that global stability must be attained, but will instead consider the necessary consequences if all synapses closely approach stability.

Absolute population stability (*maximum* or *global stability*) is reached when all synapses are either saturated or sensitive. Where $\sigma(X_jY_k)$, $\sigma(X_jX_k)$ are numbers of synaptic connections between X_jY_k, X_jX_k, these can be partitioned into fractional terms for saturated, σ_{SAT}, and sensitive, σ_{SENS}, synaptic numbers, depending on the stable end point to which the individual synapses tend in their evolution. Consequently, if $S(X_jY_k)$, $S(X_jX_k)$ are now used to represent the mean RMS variations of synaptic gain in all synapses connecting Y_k to X_j and X_k to X_j, then

$$\begin{aligned} \Psi(XY) = &\sum_{j=1}^{j=n}\sum_{k=1}^{k=n}\sigma_{\text{SAT}}(X_jY_k)S_{\text{SAT}}(X_jY_k) \\ &+ \sum_{j=1}^{j=n}\sum_{k=1}^{k=n}\sigma_{\text{SENS}}(X_jY_k)S_{\text{SENS}}(X_jY_k) \approx 0, \end{aligned} \tag{11}$$

$$\begin{aligned} \Psi(XX) = &\sum_{j=1}^{j=n}\sum_{k=1}^{k=n}\sigma_{\text{SAT}}(X_jX_k)S_{\text{SAT}}(X_jX_k) \\ &+ \sum_{j=1}^{j=n}\sum_{k=1}^{k=n}\sigma_{\text{SENS}}(X_jX_k)S_{\text{SENS}}(X_jX_k) \approx 0 \end{aligned} \tag{12}$$

defines global stability as the sum of RMS variation of all synaptic gains, which must reach zero at maximum stability.

2.3.3. Maintenance of uniform metabolic load in axons, and the densities of saturated and sensitive synapses

Grossberg and Williamson (2001), in work modeling the development of lateral and feed-forward connections within layers of the cortex, drew attention to the added constraint of metabolic requirements upon the kinds of connections which can be formed under Hebbian rules. We apply a related constraint here.

Competition occurs for metabolic resources within axons, so metabolic rate at all parts of the axonal system are approximately equal. If metabolic demands for saturated synapses are much greater than for sensitive synapses, then all cells must receive and give rise to similar proportions of saturated and sensitive synapses, the densities of

saturated and sensitive synapses respectively, must decline with distance from their cell bodies of origin, and must maintain a constant ratio. Given also that different members of $\{R(X_jY_k), R(Y_jY_k)\}$ range in value at stability from zero to some sufficiently positive value, then each cell must give rise to both saturated and sensitive synapses.

These metabolic limitations place further constraints on (11) and (12), so that

$$\sigma_{\mathrm{SAT}}(X_jY_k), \sigma_{\mathrm{SENS}}(X_jY_k), \sigma_{\mathrm{SAT}}(X_jX_k), \sigma_{\mathrm{SENS}}(X_jX_k) > 0, \tag{13}$$

$$\sigma_{\mathrm{SAT}}(X_jX_k) \propto |j-k|^{-1}, \tag{14}$$

and

$$\sigma_{\mathrm{SENS}}(X_jX_k) \propto |j-k|^{-1}. \tag{15}$$

2.3.4. Overall requirements for maximum stability

As a simple property of sums of products, for any total sum of RMS variation of synaptic gain, the terms in (12), will sum more closely to zero if dense couplings of high synaptic number are matched to low values of gain variation. That is, stability is more closely approached where

$$\sigma_{\mathrm{SAT}}(X_jX_k) \propto [S_{\mathrm{SAT}}(X_jX_k)]^{-1} \tag{16}$$

and

$$\sigma_{\mathrm{SENS}}(X_jX_k) \propto [S_{\mathrm{SENS}}(X_jX_k)]^{-1}. \tag{17}$$

However, this leads to contrasting requirements at saturated versus sensitive synapses—i.e.,

$$S_{\mathrm{SAT}}(X_jX_k) \propto R(X_jX_k) \tag{18}$$

while

$$S_{\mathrm{SENS}}(X_jX_k) \propto R(X_jX_k)^{-1}. \tag{19}$$

This means that as global stability is approached, saturated synapses linking positions more densely connected (and therefore closer together) must exhibit higher pre/post-synaptic coincidence. Conversely, sensitive synapses linking positions more densely connected (and therefore also closer together) must have lower pre/post-synaptic coincidence. These contrasting requirements impose an order upon both saturated and sensitive synapses, mapping activity in each disk to the other, in a form analogous to representation of a flat surface on a Mobius strip, as will now be shown.

2.3.5. Consequences of maximized stability at saturated synapses

We will term the configuration of saturated synapses connecting $\{Y\}$ to $\{X\}$ when stability is approached, the *input map*, and the corresponding configuration of saturated synapses within $\{X\}$ the *local map*. The input and local maps must converge to mutually compatible stable forms.

2.3.5.1. Within each disk. Saturated connections form as required by Eqs. (14) and (16), to produce the 1:1 connections.

$$X_j \to X_k, \quad \text{where } \sigma_{\mathrm{SAT}}(X_kX_j) \propto |j-k|^{-1}, \tag{20}$$

which act to enhance the initial condition Eq. (2) of inverse relationship between distance of and amplitude of synchronous oscillation

2.3.5.2. Between disks. As saturation develops in the connections mapping $\{Y\}$ to $\{X\}$, the formation of saturated connections within $\{X\}$ as required by (20) would be disrupted, unless the connections between the disks transmitted signals with cross-correlation declining with distance within the input map. Therefore, for overall stability to be approached, the input map must belong to the group of maps given by

$$\frac{Y_j^N}{|Y_j|^{N-1}} \Rightarrow X_k, \quad \text{where } \sigma_{\mathrm{SAT}}(X_kY_j) \propto |j-k|^{-1}. \tag{21}$$

Eq. (21) maps normalized distance in $\{Y\}$ to $\{X\}$, with relative angles determined by the value of N. The mapping is *continuous*, and also *complete*, since all $\sigma_{\mathrm{SAT}}(X_kY_j)$ are non-zero, as given in (13).

In an abstract mathematical sense, the input map is analogous to mapping a Euclidean plane to a Mobius plane of order N (See Fig. 2 and Appendix B). As Figs. 2 and 3 show, this abstract N:1 map corresponds to the observable form of OP response organization—but to give anatomical meaning to the connections thus described, the subscripts $j = 1,2,\ldots,n$ must be renumbered as $jm = 1,2,\ldots,n/N,\ldots,2n/N,\ldots,mn/N,\ldots,n$, where $jm = j \times m$; $m = 1,2,\ldots,N$, so that the numbering of positions on each disk is ordered into N sequential angular segments. Eq. (21) then becomes

$$\frac{Y_{jm}^N}{|Y_{jm}|^{N-1}} \to X_{km} \tag{22}$$

indicating that there are N distinct groups of neurons at all positions X_{jm}, each group receiving afferents from a distinct domain defined by angular positions in $\{Y\}$.

2.3.6. Consequences of maximized stability at sensitive synapses

The value of N is determined by the requirements for maximum stability at the sensitive synapses. This requires that the local map be compressed so as to bring the most separated points on $\{Y\}$ into closest conjunction in both the input and local maps, so that the N distinct groups of neurons at X_{jm} can then each be linked by the densest connection of sensitive synapses. Therefore the local map and the input map must have that value of N which maximizes δ, the distance over which positions jm and $j(m+1)$ in the Euclidean plane are translated to become coincident in projection to a Mobius plane of order N (See Appendix B). This is given by

$$\delta = |Y_{jm} - Y_{j(m+1)}| = 2|Y_j| \sin\left(\frac{\pi}{N}\right), \quad m = 1, \ldots, N \tag{23}$$

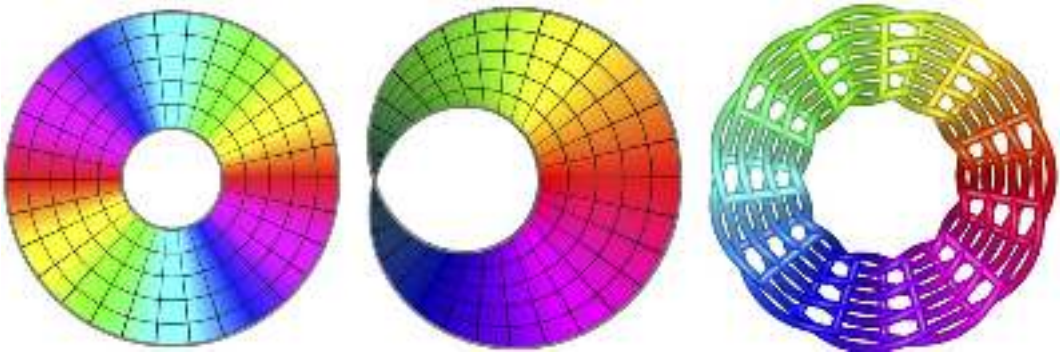

Fig. 2. Self-organization of synapses to form local maps. Left: polar plane representation of activity in an efferent field. Angles 0–2π are represented by the colors of the spectrum, repeated twice. Middle: input map; saturation of synapses projected to the afferent field forms a Mobius projection from the efferent field. Distance relations are preserved, but angular relations are doubled to 0–4π. Right: local map; synapses within the afferent field become saturated so as to form an intertwined mesh of bi-directional connections, closed over 0–4π.

Fig. 3. Transfer of the representation of moving visual objects to a local map. Left: the retinotopic representation of visual activity in V1. Black bars with arrows are matched but differently moving visual stimuli, which cross the visual field at a common position, indicated by the intermediate solid bar. The pinwheel centre is the position of the local map diagrammed in the middle image. The dotted line indicates a line symmetrically opposite the solid line, with respect to the local map. Middle: a local map representation of V1, in the form observed experimentally. The paired moving stimuli are represented at the same position on the local map, as shown by the single solid bar. Representation of the dotted line in V1 is superimposed on that of the solid line. Right: representation of the moving objects now shown as on one of the two halves ($m = 1$) of the Mobius mesh of connections, equivalent to Fig. 2, while the dotted line's representation is in the other half ($m = 2$) of the mesh.

Since δ is at a maximum for $N = 2$, this form of folding of the input and local maps maximizes stability at the sensitive synapses.

2.3.7. The emergent form of the input and local maps

Substituting the maximum of (23) into (22), and revising (20) to allow for the revised numbering convention, the input map and local maps take the form closest to global stability when

$$\frac{Y_{jm}^2}{|Y_{jm}|} \to X_{km}, \quad m = 1, 2 \tag{24}$$

and

$$X_{jm} \to X_{km}, \quad m = 1, 2, \tag{25}$$

where the density of saturated synaptic connections decreases as $|j1 - k1|$ and $|j2 - k2|$, while the density of sensitive couplings decreases as $|j2 - k1|$ and $|j1 - k2|$.

Fig. 2 visualizes the above relations. The local map is formed as an intertwined mesh of saturated couplings, closed after passing twice around the local map's centre, with sensitive synapses locally link the two turns of the mesh together. The input and local maps can, in principle, emerge with any orientation, and with either left or right handed chirality, since these properties are not constrained by Eqs. (24) and (25).

2.3.8. Mutual organization of disks

Symmetrical and all-to-all couplings between disks permit the mutual and symmetrical organization of input and local maps of each disk with respect to the other, since the requisite initial condition—the inverse relation of covariance with distance within disks, required to drive the organization of the input maps—is maintained within the evolved local maps.

2.4. Effects of variation of constraints

The two-disk model is applicable to connection systems in V1, as will next be shown—but its application requires

that the basic assumptions be relaxed in ways appropriate to each context. Changes of some of the assumptions have the following consequences:

(a) If spatial covariance is negligible, or follows a rule other than decline with distance of separation in one or both disks, the mappings described by (24) and (25), cannot emerge.
(b) If connections between disks are unilateral, then reciprocal re-modeling of each map will not take place. The efferent disk will retain its prior spatial covariance, whereas the input map and connections within the afferent disk will form as described.
(c) Where connections between $\{Y\}$ and $\{X\}$ are not uniformly dense, but are biased in density toward some sector of $\{X\}$, $\{Y\}$, this effect will skew the orientation and/or the mirroring of the map of $\{Y\}$ relative to $\{X\}$.
(d) Where signals input from $\{Y\}$ to $\{X\}$ are not spatially isotropic, but are biased toward some orientation, this effect will increase representation of lines of that orientation in $\{X\}$, and will skew the orientation and/or the mirroring of the map of $\{Y\}$ relative to $\{X\}$.

Consequences (c) and (d) can be derived by considering the effects needed to minimize all terms in (11) and (12) by similar reasoning to that applied in the standard case.

2.5. Application to V1

2.5.1. Range of application

The two-disk model is applicable to the evolution of synaptic strengths during the interaction of V1 at macroscopic scale with each macrocolumnar area, and also to interactions between respective macrocolumnar areas, as will now be described.

Application of the model in piece-meal fashion leads to solutions maximizing synaptic stability in each case, and as no contradiction arises in the various applications made, then the collective system must also achieve stability. Inter-areal cortico-cortical connections linking V1 to higher visual areas, connections between cortical layers and reciprocal interactions with the visual pathway are excluded from specific consideration in the present account. The consequences of these exclusions are deferred to the Conclusion.

2.5.2. Initial connections

We consider only projection of the visual field onto V1 via the visual pathway, and lateral connections within V1.

Two scales are naturally imposed upon this system. The ramifications of axonal branches from the lateral geniculate nucleus terminating in layer 4Cα are 300 μm diameter, matching the average interpatch distance of the long-range intrinsic connections within V1 (Blasdel & Lund, 1983; Mountcastle, 1979; Nunez, 1995). This enables us to identify a local scale—approximately 300 microns in extent, and roughly equivalent to a macrocolumn, or the breadth of an ocular dominance column—approximating a disk in the two-disk model. The global scale—V1—is subdivided into elementary units of local scale. Within the local scale surround excitation and inhibition give rise to "Mexican Hat" effects at several different scales, from a fraction of a macrocolumn to fibers spanning several macrocolumns (Bosking, Zhang, Schofield, & Fitzpatrick, 1997; Das & Gilbert, 1999; Fitzpatrick, Lund, & Blasdel, 1985; Kang, Shelley, & Sompolinsky, 2003; Liley & Wright, 1994). At all scales these systems are capable of supporting fields of synchronous oscillation. At the global scale, polysynaptic connections link individual macrocolumns to the activity over much of V1 (Braitenberg, 1978; Braitenberg & Schuz, 1998).

The initial condition for the system (corresponding to that during embryogenesis) is one of diffuse connections.

Subsystems required for description are:

$\{Q_j\}$; $j = 1 \ldots n$; receptive fields in the visual plane.
$\{P_{jm}\}$; $jm = 1,2,\ldots,j1,\ldots,k1,\ldots,n/2,\ldots,j2,\ldots,k2,\ldots,n$; the corresponding organization of projections of the receptive fields toV1.
$\{p_{jm}\}$; elements of $P_0 \in \{P_{jm}\}$, which will become organized into local maps.
$\{p'_{jm}\}$; elements of local maps at P', the neighbors of P_0.

2.5.3. Evolved connections

Final maps of saturated connections are listed in Table 1, and the processes leading to the emergence of these maps are discussed in the following sections.

2.5.4. The classical receptive field (cRF) and local maps

Direct axonal projections of the visual pathway cannot be assumed to transfer signals in which spatial covariance declines with distance. The two-disk model is not applicable, in accord with (a) in Section 2.4. Feed-forward spatial filter models appear more appropriate, such as the work of Ernst, Pawelzik, Sahar-Pikielny, and Tsodyks (2001) which shows that feed-forward Hebbian processes can impose OP on cortex.

Feed-forward models and the present model have an important correspondence in one respect. Spatial filter models treat the rotation of a straight line through $0-\pi$ radians as aliased by rotation through $\pi-2\pi$, and in dimensional models a similar effect gives rise to the angle-doubling of OP about a singularity. The same angle-doubling effect is seen in the two-disk model. Consequently co-incident synaptic representation of OP via feed-forward connections and OP responses mediated via lateral connections (as described in the following sections) is topologically possible. While cRF fields need not correspond precisely to emergent local maps, overlap must occur if connection scales are similar. Co-incident representations also imply that cRF fields are modulated by lateral interactions.

Table 1
Emergent saturated connection maps

Anatomy	Map	Connection characteristic
Visual pathway	$Q_j \rightarrow P_k\ j \approx k$	cRF spatial filter with angle-doubling for OP
Transmission within V1 by polysynaptic pathways	$\frac{P_{jm}^2}{\lvert P_{jm}\rvert} \rightarrow p_{km}; \frac{p_{jm}^{1/2}}{\lvert p_{jm}\rvert^{-1/2}} \rightarrow P_{km}$	Input and output bi-directional connections from V1 to each macrocolumn. $\sigma_{\mathrm{SAT}}(p_{km}P_{jm}) \propto \lvert jm - km\rvert^{-1}$
Long intracortical connections	$p_{jm} \rightarrow p'_{km}; p'_{jm} \rightarrow p_{km}$	Connections between local maps oriented as mirror-images $\sigma_{\mathrm{SAT}}(p_{km}p'_{jm}) \propto \lvert jm - k'm\rvert^{-1}$
Short intracortical connections	$p_{jm} \rightarrow p_{km}$ and $p_{km} \rightarrow p_{jm}$	$\sigma_{\mathrm{SAT}}(p_{km}p_{jm}) \propto \lvert jm - km\rvert^{-1}$

2.5.5. Interaction of V1 with each local map via polysynaptic routes

2.5.5.1. Relation of local and global maps. Beginning from the initial conditions, the two-disk model can be applied to extended V1 (the $\{Y\}$ disk) acting upon any given cortical area of approximately 300 microns diameter (the $\{X\}$ disk). We first consider the interaction of the whole of V1 with a single local map, confining attention to the unioccular case. Activity throughout the extent of V1 conforms to the distance/covariance relations assumed in the two-disk model, for an additional reason to the variation of synaptic density with range—viz: spatial covariance in visual stimuli generally declines with increasing distance. Synchronous fields generated in V1 can spread over polysynaptic pathways to the local map, so the two-disk model is applicable under the restriction (b) of Section 2.4. The spread of signals over polysynaptic pathways is considered, at first approximation, to meet the assumption of a uniform and all-to-all input, from V1 to the macrocolumnar sized area, which will become the local map. Therefore we expect emergence of a retinotopic map folded into the Mobius configuration within each macrocolumn. Input from the global field to the local map is approximated by

$$\frac{P_{jm}^2}{|P_{jm}|} \rightarrow p_{km} \tag{26}$$

and return connections throughout V1 must follow the inverse map

$$\frac{p_{jm}^{1/2}}{|p_{jm}|^{-1/2}} \rightarrow P_{km}. \tag{27}$$

The return connections are necessarily weak, and cannot alter the retinotopic ordering of V1.

Extending consideration to the binocular case, where visual input from both eyes reaches areas within V1, the assumption of stochastic dependence of spatial covariance versus distance in the stimulus field breaks down, leading to failure of the model in accord with (a) of Section 2.4. Further consideration of this special case is deferred to Section 3.2.

2.5.5.2. Object representations, effect of lags, OP, and DP. The local map permits moving objects in the visual field to produce specific moving patterns of neuronal activity within each local map (See Fig. 3). This effect follows from the retinotopic organization, in Mobius configuration, which arises within the local map purely from the inverse distance/covariance relation in the inputs, and requires the inputs to have only white or brown spatial noise structure. Once this retinotopic projection has developed, further evolution of local connections under the influence of specifically structured visual stimuli will permit conditional probabilities to be represented in the local map, as follows.

The retinotopic ordering requires that some point on the local map must correspond to the position of the local map upon the global map. As indicated by the circular graphical origins in Fig. 2, the position p_0 corresponds to P_0 on the global map. Lines radiating from p_0 must correspond to lines oriented at all angles in the cRF. Therefore spatial filtering on the input pathway will lead to the production of an OP singularity at p_0, by transfer of covariances in the global map to the local map. In the same way, continuity of OP will extend from the singularity outwards into the local map.

Against this primary spatial ordering, specific object information can then be relayed. The map $O(q,t-\tau) \rightarrow O(P,t)$ describes relay of information concerning a visual object, $O(q,t)$ in the visual pathway, where τ is a spatially uniform delay. Introducing time lags required for synchronous relations to be established between points on the global and local maps, and substituting $jm = km$ in Eq. (26) so as to indicate the pattern of highest density input connections to each local map, we can write:

$$O\left(\frac{(P)^2}{|P|}, t - \frac{|P|}{v}\right) \Rightarrow O(p,t), \tag{28}$$

where $\frac{|P|}{v}$ is the axonal conduction delay (essentially equal to the time to establish synchrony) for signals relayed from position P in V1, to the local map situated at $P_0 = 0$, and v is axonal conduction velocity. Note that this object mapping is 2:1 as a consequence of the folding of the image of V1 into Mobius form, as shown in Fig. 3, and thus corresponds to the form observable by voltage-sensitive dyes and related experimental methods.

An object representation, $O(p,t)$, can be generated by either of visual objects traveling in roughly opposite direc-

tions, which relay signals to the same position on the local map. Designating these dual objects as $O^+(P,t)$, and $O^-(P,t)$, the relay of their images to the local map are described by

$$O^+\left(\frac{(P)^2}{|P|}, t-\frac{|P|}{v}\right) \Rightarrow O^+(p,t), \quad O^-\left(\frac{(P)^2}{|P|}, t-\frac{|P|}{v}\right) \Rightarrow O^-(p,t). \tag{29}$$

Local waves generated within the local map by each object's passage differ, and consequently evolution of distinct patterns of local connectivity will then develop, thus representing contingent probabilities associated with selective responses to particular objects and motions. Depending on linkages of neurons in the local map associated with $O^+(p,t)$ or $O^-(p,t)$ neurons may respond selectively to objects with separate directions of movement. Direction preference (DP) can thus be represented as

$$DP(p) = O^+(p) - O^-(p). \tag{30}$$

2.5.6. Interaction between neighboring local maps via monosynaptic routes

In isolation local maps would arise with random chirality and orientation. However, the consolidation of their input synapses is also subject to interactions between the local maps, mediated by local intra-cortical axons of greater length than the diameter of the local map. For the long intra-cortical connections an inverse synaptic density/range relation holds, similar to distance and densities within each local map. Inter-map connections conform to the two-disk model, apart from the added feature that adjacent maps form interconnections with each other with synaptic densities which decline with distance, rather than being uniform density all-to-all connections, so connections between local maps have the form

$$p_{jm} \rightarrow p'_{km}, \quad \text{where } \sigma_{SAT}(p'_{km}p_{jm}) \propto |p_{jm} - p'_{km}|^{-1} \tag{31}$$

in accordance with condition (c) of Section 2.4. Consequently, synaptic stability is maximized when adjacent local maps are arranged so that each local map forms a mirror-image of its neighbor and the local maps pack in an hexagonal array. Since each local map has six neighbors, their orientations and chirality must minimize the departure from mirror orientation in each direction. Fig. 4 shows the principles of alignment of adjacent local maps.

The couplings between local maps, once they have emerged, are well suited to mediate relay of large-scale synchronous fields throughout V1 by polysynaptic pathways.

Long-range inhibitory connections have been neglected in this account. We suppose that inhibitory connections are not subject to Hebbian modification, but vary in strength conversely to the strength of excitatory connections. Thus, long-range inhibitory connections would link neurons in each local map having low coincidence with each other.

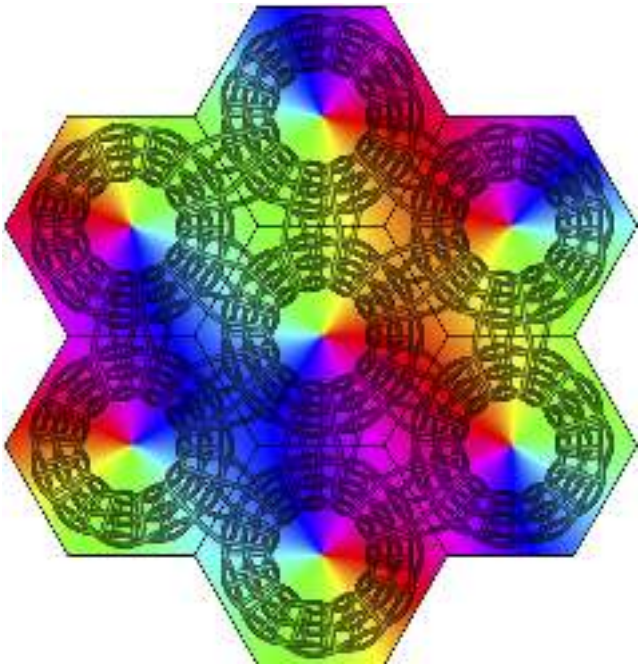

Fig. 4. Stable relations among adjacent local maps. Each local map has orientation and has chirality such that the central local map is surrounded on each side by maps approximating mirror images of the central map. Saturated synaptic connections between maps join homologous positions.

2.5.7. Polysynaptic interactions of local maps during early stages of synaptic evolution

During the maturation of the local maps some will reach their stable form earlier than others because of stochastic variations of all sorts. In addition to the monosynaptic intra-cortical interactions between maps described above, the more mature local maps will exert a biasing influence, by polysynaptic routes, upon parts of V1 at an earlier maturational stage. The random orientations of the relatively mature groups of maps, upon the sites of maps yet to form, will lead to a biasing of orientation and chirality in the immature maps which is described by condition (d) in Section 2.4. This influence is further discussed and modeled in Section 3.1.

3. Comparisons with experimental data

3.1. Singularities, linear zones, saddle points, and intrinsic fibers

The organization of OP in V1 is similar to that shown in Fig. 4, but is more disorganized than the symmetrical structures shown. We modeled the development of OP local maps in simulations designed to show the way that the emergence of many local maps, interacting with each other while individually evolving to a stable end-point, would give rise to distortions from the idealized case—a process analogous to that of irregular crystal formation. This procedure also permitted comparison to maturational changes in the newborn.

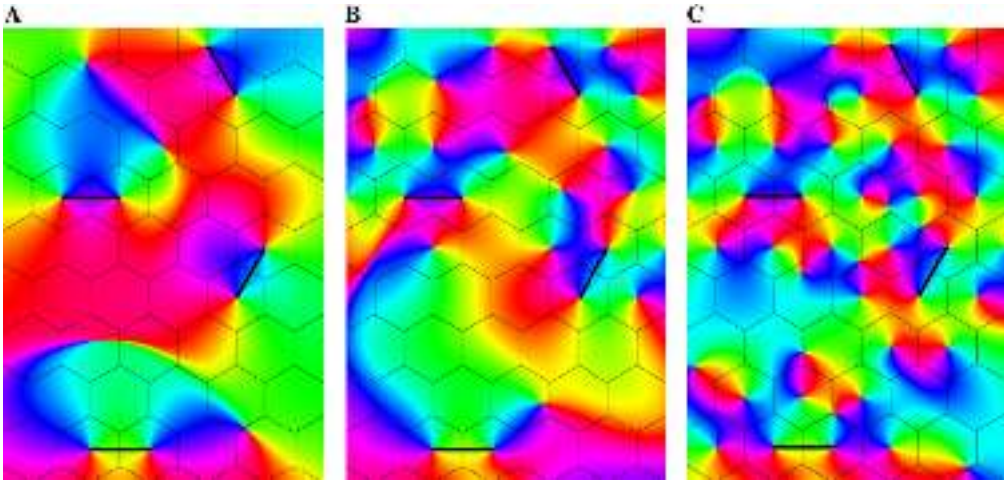

Fig. 5. (A) Early development of OP. Black bars indicate early pairs of local maps with mirror-image symmetry. Between these maps the initial OP of cells is biased by the influence of the early maps. (B) Later, more completed local maps have formed up adjacent to the early maps. The expanded set of complete local maps continues to bias the orientation and chirality of emerging maps.(C) Continuation toward the completed state shown in Fig. 6A.

Figs. 5A–C, show stages in the simulated evolution of OP in V1.

As the initial condition (Fig. 5A) pairs of adjacent mirror-image color-wheels were placed in random positions in the frame, as indicated by the solid black lines. These initial pairs represent local maps that have developed early, under strictly local influence, in conformity with the processes diagrammed in Figs. 2 and 4. These pairs then seed subsequent organization amongst later evolving local maps, via a two-phase process, as initially discussed in Section 2.5.7. (See Appendix C for further details.). The first phase is the induction of preference for a particular orientation and chirality in emerging maps in the surrounding field, induced by the average of the activity in the wider field. This field effect is given by vector summation of OP in the completed local maps, conveyed throughout the field of V1. The second phase is the final allocation of orientation and chirality of later emerging maps, placed sequentially about each of the seeding pairs, with their chirality and orientation chosen to minimize disparity of OP at the interfaces of each local map. Since the two phases correspond roughly to the earlier and the later stages of local map evolution, temporal smoothing of the evolving field provided continuity. Propagation of newly completed local maps outwards from initial seed-pairs maps ultimately results in intersection of sets of local maps for which no very close mirroring of adjacent maps was possible, as is seen occurring in Figs. 5B and C, and in final form in Fig. 6A.

This procedure reproduces typical features of orientation preference maps, as can be seen by comparison of simulated (Fig. 6A) and real data (Fig. 6B). Linear zones, saddle points, and occasional additional aberrant singularities (which do not correspond to centers of local maps) appear as junctions where differently seeded zones intersect, while preservation of some of the idealized orderly mirroring diagrammed in Fig. 4 is seen in both real and simulated data.

As discussed earlier, mutual organization among local maps as diagrammed in Fig. 4 results in saturated synaptic connections between homologous points. In accord with this expectation, linkage between cells of similar orientation preference should occur between local maps (Malach, Amir, Harel, & Grinvald, 1993; Yoshioka, Blasdel, Levitt, & Lund, 1996), and is known to do so in fact, as is shown in Fig. 6B.

The emerging form of OP in Fig. 5 is plausibly comparable to experimental data. In newborn ferrets, Chapman, Stryker, and Bonhoeffer (1996) showed that the detail of OP resolution increased rapidly in early post-natal life. The earliest maps seen were low-contrast, with regions of orientation-specific activity that were difficult to distinguish from noise. In our simulations the large areas of continuous OP seen in Fig. 5A are associated with low vector magnitudes, and would be obscured by the presence of noise. The early maps matured over a period of several days into the high-contrast, patchy maps typical of adult animals, and the structure of the orientation maps was remarkably constant over time. The indistinct features in the earliest maps were always patches of the same sizes and shapes and at the same locations as in the maps obtained in subsequent recording sessions. Details of the more mature maps, including the relative intensities of individual iso-orientation domains, were also constant from one recording session to another over periods of several weeks. This relative constancy of local maps once their emergence has begun is also seen in our simulations.

Our simulations are limited, in that they do not describe the full process of synaptic consolidation, but instead rely on temporal smoothing of early and late dynamical states, and on predicted topological relations of the emergent maps. Also they do not include features of evolution of feed-forward connections in the visual pathway. However, the comparative realism of the results may indicate that

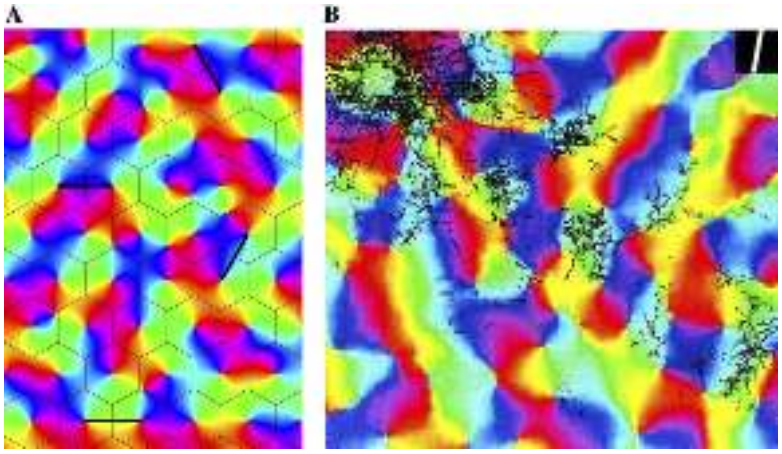

Fig. 6. (A and B) Simulated and real maps of orientation preference. (A) Final configuration of OP consequent to seeding the development of fields of OP with the local map mirror-image pairs shown joined by solid lines. (B) Real OP as visualized in the tree shrew by Bosking et al. (1997). Intracortical connections superimposed in black connect zones of like OP.

evolution of feed-forward connections is synergic with that of lateral connections.

3.2. Ocular dominance columns

Organization of OP into ocular dominance (OD) columns has been described by Swindale, Shoham, Grinvald, Bonhoeffer, and Hubener (2000), among others. Adjacent macrocolumns responsive to either the left or right eye alternate, organized into parallel columns for each eye. Singularities tend to lie at the centers of each OD column, and OP linear zones cross the boundary between OD columns orthogonally to the boundary.

The visual information delivered to V1 from the two eyes arises from overlapping projections of the visual field because of the lateral separation of the eyes. Their co-ordinated visual scanning also introduces a spatio-temporal lag covariance in the signals transmitted from each eye. Consequently, the assumption made for the uniocular case, that spatial cross-correlation is a declining function of distance of separation, is not valid. In this altered circumstance maximum stability may be reached by suppressing input from opposite eyes in adjacent local maps, each sharing closely similar inputs, and individually conforming to the inverse distance/covariance relation. Synergic linkage between adjacent maps will then follow a modification of Eq. (31)—i.e.,:

$$p_{jm} \rightarrow p'_{km}, \quad \text{where } \sigma_{\mathrm{SAT}}(p'_{km}p_{jm}) \propto |jm - (k+d)m|^{-1}, \tag{32}$$

where d is a distance determined by lagged covariance of the twin signals. Maximization of stability is then achieved if all the local maps are now arranged as mirror images of their neighbors, directed in radial bands outward from the foveal point, since the disparities d are oriented in the major axes of visual scanning. Pairs of adjacent maps with opposite OD preference will form with radial symmetry —and synergy between homologous points will now occur optimally within a square, rather than an hexagonal, symmetry.

The same algorithms as applied to form Fig. 6A have been used to form Fig. 7A—but in this case dual local map pairs with mirror image symmetry were placed in horizontal positions with square symmetry, creating columns. Subsequent development of intervening local maps was then simulated in the same way. The result is a more orderly and systematic mirroring of local maps in alternate columns throughout—with alignment of singularities down each OD column, and orthogonal crossing of OP between OD columns, as described experimentally by Obermayer and Blasdel (1993).

Support for a contribution to the formation of OD columns by this mechanism comes from the finding of enhanced definition of OD columns in animals with severe strabismus imposed during visual development, since this would increase ocular disparity. However, the incompleteness of this explanation is apparent from the persistence of some OD structure in animals raised with bilateral eye closure (Kandel & Schwartz, 1985).

3.3. Object velocity, object extension, and orientation preference

Using moving texture stimuli and optical imaging, Basole et al. (2003) recorded OP in populations of cells and single cells, as a function of stimulus velocity, direction of motion relative to orientation, and length, of small texture elements. All these variables caused apparent OP to differ, in contrast to findings with conventional, laterally extended, grating stimuli. We propose that these findings can be explained by a modulation of the cRF OP response by conditioning signals transferred to the local map from surrounding V1.

In Fig. 8, P_a and P_b are two points in V1 which are activated by a texture element, $P'_aP'_b$ moving with a velocity $\mathbf{v}$, with an orientation ω relative to the direction of motion, such that, by continued element movement, $P'_aP'_b$ will straddle the local map situated at P_0, thus facilitating a maximal

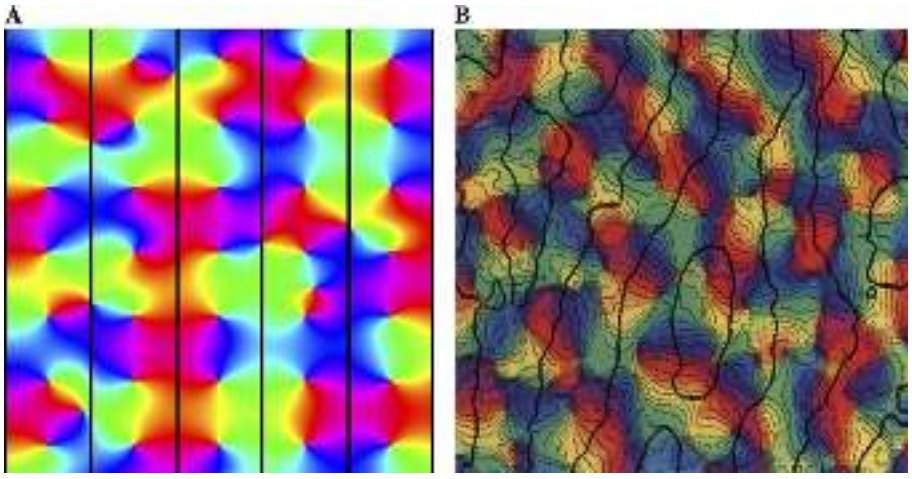

Fig. 7. (A) Results of simulating the development of OD columns. (B) Real OD columns, as visualized by Obermayer and Blasdel (1993).

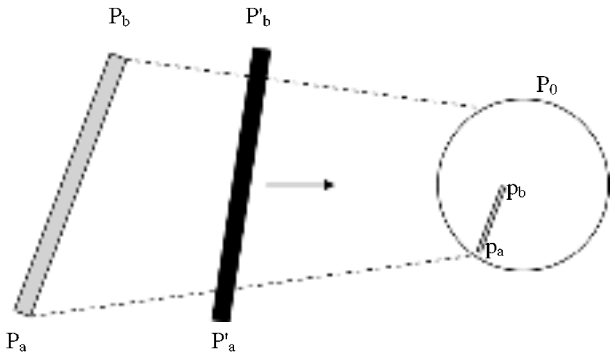

Fig. 8. Conditioning of receptive field OP by moving textures. Grey semitone bars, P_aP_b and p_ap_b represent corresponding positions in the global and local maps respectively. The black bar $P'_aP'_b$ is a texture element moving to straddle the local map at P_0, and which has crossed P_a and P_b so as to generate *trans*-cortical signals which reach P_0 simultaneously.

response to the stimulus received from the cRF, which arrives at P_0 soon after the relay of signals to P_0 from P_a and P_b. Because of conduction delays $v\Delta t$, activity in the local map at $p_ap_b(t)$ is generated by signals at P_a at $t - \frac{|P_a - P_0|}{v}$, and at P_b at $t - \frac{|P_b - P_0|}{v}$. Apparent OP experimentally observed at p_ap_b is measured as functions of the velocity, orientation and extension of $P'_aP'_b$ that is required to deliver simultaneous signals to p_ap_b.

Appendix D gives a geometrical argument based on Fig. 8, to show that $\Delta\psi$, the change in apparent OP, is given by

$$\Delta\psi = \sin^{-1}[\sin(\pi - \omega)\left|\frac{\mathbf{v}}{v}\right|(|P_a - P_0| - |P_b - P_0|)/|P_a - P_b|]. \quad (33)$$

The results of Basole et al. can then be summarized and explained by application of (33):

- When texture elements are oriented at right angles to their direction of motion, no effects on OP is observed, and results resemble those for conventional grating stimuli. This is the case where $\omega = \pi/2$, so $P'_aP'_b$ and P_aP_b are parallel, therefore $|P_a - P_0| = |P_b - P_0|$, and $\Delta\psi = 0$.
- When texture elements are oriented at opposite senses to the axis of motion, the changes in OP are equal but opposite. Equivalently, with change of the angle of attack from $+\omega$ to $-\omega$, since $\sin(\pi - \omega) = -\sin(\pi + \omega)$, $\Delta\psi$ will have equal magnitude, but opposite sense.
- As the length of texture elements is increased, the magnitude of changes in OP are diminished, and results again resemble those for conventional gratings. This is the case where $|P_a - P_b|$ tends large. Consequently, $[|P_a - P_0| - |P_b - P_0|]/|P_a - P_b|$ decreases in magnitude, therefore $\Delta\psi$ tends to zero.
- As the velocity of movement of the texture elements is increased, change in OP increases in magnitude roughly proportionally to the increase in velocity. Since $\Delta\psi$ is roughly proportional to $|\mathbf{v}|$ in (33) this result is also as expected.

The applicability of Eq. (33) has a limit where $|\mathbf{v}| = \frac{|P_a - P_b| \times |v|}{(|P_a - P_0| - |P_b - P_0|)\sin(\pi - \omega)}$, since $\sin\Delta\psi$ cannot exceed unity. This limit of applicability is reached when the stimulus bar passes at such a high angle that it does not pass over the receptive field of P_0. Further, where $|\mathbf{v}|$ approaches $|v|$, the concept becomes invalid, since the stimulus representation in V1 would overtake the propagating wave front. The findings of Basole et al. suggest an asymptotic limit is approached at high stimulus velocities, but this effect has not yet been systematically studied.

3.4. Direction preference and fractures

The occurrence of "fractures"—sudden reversals in DP—has been observed by Weliky, Bosking, and Fitzpatrick (1996), and by Swindale, Grinvald, and Shmuel (2003). DP fractures have been demonstrated in the primary visual cortex of the cat and the ferret, although in the monkey strong preferences for direction of movement are not apparent in optical imaging maps (Swindale et al., 2003; Weliky et al., 1996). The species specificity may reflect the functional importance of movement

detection in nocturnal predators. DP and OP angles are generally orthogonal, and DP fractures emanate from orientation preference singularities. Swindale et al. (2003) have observed that the number of fractures per singularity is always an odd number—usually one. The occurrence of odd numbers of fractures can be explained as a consequence of the Mobius configuration of saturated connections

Modifying Eq. (30) for DP to represent specific positions within the Mobius disk connection mesh,

$$DP(p_{jm}) = O^{+}(p_{jm}) - O^{-}(p_{jm}), \quad m = 1, 2. \tag{34}$$

The representations of O^{+} and O^{-}, respectively, are each Mobius projections from their positions on the global map.

The DP fracture, $F(p_{jm})$, is a line radiating from the singularity at some angle ϑ on the range 0–2π, for which $DP(p_{jm}) = 0$. Therefore the inverse map

$$\frac{F(p_{jm})^{1/2}}{|F(p_{jm})|^{-1/2}} \rightarrow F(P_{jm}) \tag{35}$$

describes a line $F(P_{jm})$ in the global map surrounding P_0, for which response to moving objects shows opposite preference on opposite sides of the line. Using a continuous labeling for directions +, −, the reversal of DP with respect to O^{+} or O^{-} at this line is in the opposite sense on opposite sides of $F(P_0)$.

As shown in Fig. 9, the line $F(P_{jm})$ as represented at the DP fracture, requires responses to O^{+} and O^{-} to change their relative dominance consistently at the angles 2ϑ and $2\vartheta + \pi$ (on the range 0–4π) within the local map. Therefore, with respect to the mapping of either O^{+} or O^{-}, the DP fracture is analogous to a cut-and-reverse join in a Mobius strip. To maintain closure and continuity a Mobius strip must have an odd number of cut-and-reverse joins. Therefore the number of DP fractures in a local map must be odd.

A related topological argument for the occurrence of only odd numbers of fractures is discussed in Swindale et al. (2003). Their argument rests upon continuity properties and requires a priori assumption of the form of OP around singularities, and is therefore consistent with feed-forward spatial-filter models. Our argument shows that lateral interactions can order DP in a form compatible with the feed-forward account.

4. Conclusion

We have shown that V1 response properties may arise from Hebbian learning with decay when a stable configuration is achieved via lateral interactions. Effects of object velocity, orientation and extension which are not explained by feed-forward models are accounted for, yet there is no contradiction with the principles of feed-forward modeling and the two approaches appear to be complementary.

Our explanation generates continuity and completeness in a similar way to dimensional models, since these topological properties are transferred from the global to the local maps, and is consistent with theoretical considerations regarding synchrony, contextual learning and the coherent infomax criterion (Kay & Phillips, 1997; Phillips & Singer, 1997). That is, that learning rules of this type, coupled to a mechanism of synchrony, can lead to maximization of information storage in neural networks. It now appears that this maximization of information storage implies the development of realistic anatomical features, further validating the realism of such types of learning rule. Of central importance to this model is the way in which synapses are assumed to achieve stability with a substantial proportion of synapses remaining in the sensitive state. While this assumption is essential for the model to be applicable to short-term learning, it is not essential for long-term consolidation of synaptic couplings. If short-term learning has established the framework of synaptic

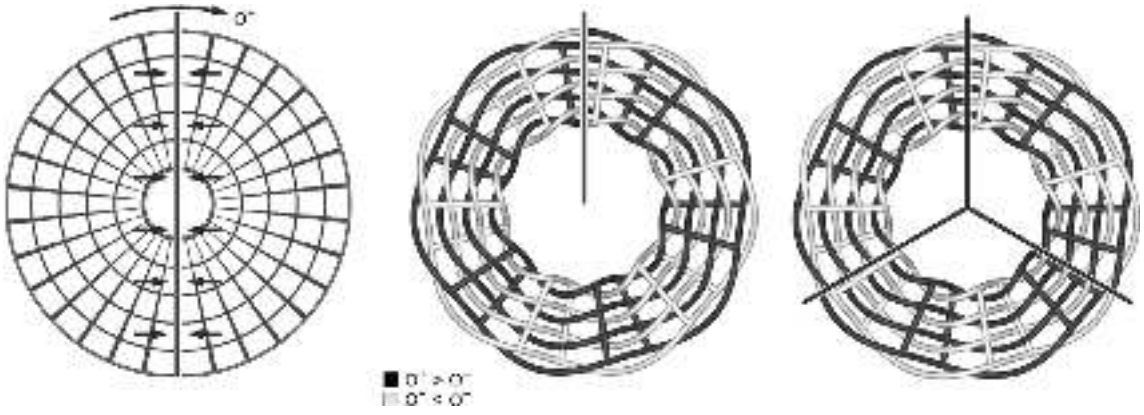

Fig. 9. Proposed origin of direction preference fractures. Left: a field of V1 projecting to a local map located at the centre of the field. Preferential response to moving objects is reversed along an axis of the V1 field, indicated by oppositely directed arrows. A visual stimulus, O^{+}, transiting the axis, exhibits reversed changes in preferential response on opposite sides of the V1 field. Middle: projection of direction preference to the local map. White and black wiring now show the location of inputs from opposite sides of the axis in V1. Consistent reversals of direction preference for O^{+} projected from opposite sides of the V1 field occur at the vertical black line, forming a DP fracture. Right: multiple fractures are possible only if the total number fractures is odd.

strengths, slow consolidation could proceed in saturated synapses, leading to permanent structural change, while sensitive synapses might wither to nothing. Biochemical and anatomical differences in long-term versus short-term memory, and synaptic pruning, might therefore be introduced into the model.

A novel aspect of our proposal is that a meshwork of saturated synapses analogous to a Mobius strip emerges within each local map. This pattern of connectivity has not been anatomically or physiologically directly detected, but since the connection meshwork would necessarily be very fine-grained there is no reason to expect it to be readily demonstrable.

According to our account, local maps achieve their distance metric from statistics of the stimulus field and of the fields of synchronous oscillation, and secondarily develop more detailed structure from details of specific visual objects. This may explain why the visual cortex appears poorly organized at birth and when deprived of visual input and exhibits greater resolution with increased exposure to visual stimuli (Blasdel & Lund, 1983; Chapman et al., 1996; Kandel & Schwartz, 1985; LeVay, Wiesel, & Hubel, 1981; Ruthazer & Stryker, 1996). The structure of input signals would need to be only white or brown spatial noise, to begin the organization of maps similar to those later observed in the mature, trained, cortex. This explanation is also compatible with the results of more selective visual deprivation (Blakemore, 1976; Blakemore, Movshon, & Sluyters, 1978; Peck & Blakemore, 1975). If no visual stimuli constructed of horizontal lines were ever seen, then no local map intra-cortical connections corresponding to horizontal lines would result. Conversely, it is apparent from other experiments that innate factors contribute, outside the scope of this and other learning based models. For instance, binocular columns appear even in the absence of visual inputs (LeVay et al., 1981) and so the mechanism for OD column formation we have suggested can play only a supportive role in the emergence of the adult structure.

Our account is, in principle, subject to further experimental tests. Although analysis of connections using electrophysiological estimates of synaptic gain might reveal the Mobius meshwork connection pattern, this appears a demanding task. It may be more practical to attempt demonstration of the symmetrical folding of the V1 field within the local map, as diagrammed by solid and dashed lines in Fig. 3. Cells closely located to one another, but responsive to stimuli positioned on opposite sides of the cRF, ought to be demonstrable. Eq. (33) suggests the possibility of quantitative testing of the effects of object velocity on OP in conditions in which all terms in the equation are precisely specified. Our account of the findings of Basole et al. (2003) also has features in common with the model advanced by Series et al. (2002) to account for orientation-dependent modulation of apparent speed and unification may be possible. Third, our proposal raises the possibility that other features in the global V1 map may find representation in local maps. We have earlier suggested (Alexander et al., 1998) that CO blobs might fill the role of representation of the macular region. However, present evidence is not sufficient to determine the extent of V1represented in local maps.

The self-organizing principles applied here to V1 may have generality beyond the primary visual cortex to that of interaction between cells at other stages of cortical vision, and to cortical processing in general. The relationship between spatial separation and covariance pertaining to visual images may be transformed to other metrics than physical distance in other sensory modalities, and at other hierarchical levels, but since axo-synaptic connection densities decline with distance on almost all spatial scales of the brain (Braitenberg, 1978; Braitenberg & Schuz, 1998) then the covariance/distance relations from which the synaptic maps emerge may have wide currency. Similar principles may apply to the relationship of V1 with higher visual areas—a problem deferred from consideration in this paper. Since all visual areas are reciprocally and richly interconnected, their joint synaptic stability might emerge by processes analogous to, but on a larger scale than, those leading to the mutual organization of local maps.

The discrete macrocolumnar structure of V1 is not apparent more widely in cortex, and this may be because of the need for the local maps in V1 and the discrete cRF connections to conform, while elsewhere, the equivalents of local maps might intermingle. The occurrence of topologically identical representations at local and global levels may also be relevant to the occurrence of interactions between scales, and between small local neural networks operating co-operatively at wide separations in the brain.

Acknowledgments

We thank the Oakley Foundation for financial support, and our colleague Dr C. J. Rennie, of the Department of Physics and the Brain Dynamics Centre, University of Sydney, for helpful discussion.

Appendix A. Wave properties underlying synchronous oscillation

Electrotonic and pulse activity in the cortex can be treated as activity in a wave medium (Chapman et al., 2002; Freeman, 1975; Haken, 1996; Jirsa & Haken, 1996; Rennie et al., 2000; Robinson et al., 1998; Wright, 1997; Wright et al., 2000). A suitable wave equation (Robinson et al., 1998) is

$$\left(\frac{\partial^2}{\partial t^2}+2\gamma_{e,i}\frac{\partial}{\partial t}+\gamma_{e,i}-\upsilon^2\nabla^2\right)\phi_{e,i}(p,t)=\gamma_{e,i}Q_{e,i}(p,t), \qquad \text{(A1)}$$

$\gamma_{e,i}$ is the characteristic range of excitatory and inhibitory intracortical axons, respectively, υ is the local velocity of axonal conduction, p is vector position on the cortical surface, t is time, $\phi_{e,i}$ is the normalized synaptic flux at

excitatory and inhibitory synapses, and $Q = Q_{e,i}$ represents the firing rate of excitatory and inhibitory cells. Auxiliary equations are

$$Q_{e,i} = Q_{e,i}^{\max}/(1 + e^{-\pi(V_{e,i}-\theta_{e,i})/\sqrt{3}\sigma_{e,i}}), \tag{A2}$$

$$V_{e,i}(p,t) = \sum_{(q=e)\wedge(q=i)} g_q \left[\frac{ab}{b-a}(e^{-a\tau} - e^{-b\tau})\right] \otimes [\varphi_q + \Phi_q](p, t-\tau), \quad t \geqslant 0,$$

where $Q_{e,i}^{\max}$ are maximum action potential rates, $V_{e,i}$ are dendritic field potentials, $\theta_{e,i}$ and $\sigma_{e,i}$ are distribution parameters of firing-probability squash functions, $g_{e,i}$ are aggregate synaptic gains, α, β are time-constants, and $\Phi_{e,i}$ are synaptic flux inputs from external sources.

Experimental observations (Steriade, Timofeev, & Grenier, 2001) show action potential rates in alert cortex average about 20 sps, and vary in rate much less than the full range of firing rates possible for driven neurons. Simulation of activated cortex associates the comparatively stable firing rate with a transitional state, balanced between dissipative and generative modes of neural activity (Wright et al., 2003).

In common with all additive delay networks, the cortical wave medium selectively rejects inverse-phase ("odd") components in spontaneous or induced activity in all bi-directionally coupled excitatory elements, and selectively retains in-phase ("even") components (Robinson et al., 1998; Chapman et al., 2002), producing synchronous oscillation, and at the local map scale the relative density of excitatory and inhibitory synapses produces greater synchrony magnitudes at shorter ranges.

Appendix B. Properties of the Mobius plane

B.1. Definition of Mobius plane

We define a Mobius plane, $\{\hat{X}_j\}$, of order N ($N + ve$) as an abstract plane which is a generalization of a Mobius strip, and is a simple example of a Riemann surface. Positions on the plane are given by the complex variable $\hat{X}$, which has common reference zero to a Euclidean plane $\{X_j\}$, where

$$j = 1, 2, \ldots, n,$$

$$|X_j| = |\hat{X}_j|, \tag{A3}$$

$$\pm N \arg X_j = \arg \hat{X}_j, \tag{A4}$$

where $\arg X_j$ has the range 0–2π, $\arg \hat{X}_j$ has the range 0–2Nπ and ± indicates that the Mobius plane may have left or right chirality.

B.2. Projection to the Mobius plane

The N:1 map

$$\frac{X_j^N}{|X|_j^{N-1}} \Rightarrow Y_j \tag{A5}$$

is a projection of the Euclidean $\{X_j\}$ upon a second Euclidean plane $\{Y_j\}$. Renumbering $j = 1, \ldots, n$ as $jm = j \times m, j = 1,2,\ldots,j,\ldots,n/N$ and $m = 1,2,\ldots,N$ so that the subscript m defines an angular sector about the origin of $\{X_j\}$, then

$$\frac{X_{jm}^N}{|X|_{jm}^{N-1}} \to Y_{jm} \tag{A6}$$

is the projection of a Euclidean plane to a Mobius plane.

The map (A5) compresses the representation of points X_{jm} and $X_{j(m+1)}$ within $\{Y\}$ to co-incidence. The distance of translation to co-incidence, δ, is found by plane trigonometry to be

$$\delta = |X_{jm} - X_{j(m+1)}| = 2|X_{jm}| \sin\left(\frac{\pi}{N}\right). \tag{A7}$$

Appendix C. Simulation of maturation of OP

Simulation of the evolution of OP was performed on a virtual plane of pixels, with hexagonal elements partitioning the plane. Each element ultimately becomes the locus of a local map, with a color pinwheel, centered at the singularity within each element.

For simplicity, we assumed an initial condition arising from the random placement of several pinwheels, in mirror-image pairs, as indicated by the black bars in Fig. 5A. These "seeding" map pairs were located randomly and varied between simulations.

From the initial condition, two distinct, but complementary processes, which approximate early and late phases of interaction among evolving local maps, were applied.

C.1. Early phase: Field effects on the surround exerted by completed maps

Seeding maps were ascribed a vector of unity magnitude, and an orientation angle (appropriately colored) and a mirror state as follows: The ith "seeding" map M_i is characterized by:

(x_i,y_i)	the position of the centre of the pinwheel on the continuous plane
ϑ_i	the angle of the pinwheel, 0,…,2π
m_i	the mirror state, ±1.

From the initial condition a vector was calculated for every other pixel in the field, which was the vector average of the seeding maps, weighted by scalar value $1/d^n$, where d is the distance between each pixel and the ascribed pixels, and n is a parameter which was varied from 1 to 3 in successive simulations, to ensure that no essential property of the simulation was sensitive to the degree of weighting.

The unit vector at any point (pixel) on the plane (x, y) due to the ith pinwheel/map is

$$P_i(x,y) = P(m_i\cos(\vartheta_i + \alpha_i), \sin(\vartheta_i + \alpha_i)),$$

where α_i is the angle of the vector $(x - x_i,\ y - y_i)$ in the range $0,\ldots,2\pi$. The vector P at position (x,y) is the sum of the weighted contribution over all p pinwheels/maps

$$P(x,y) = \sum_i P_i(x,y)/((x-x_i)^2 + (y-y_i)^2)^{n/2}, \quad i = 1,\ldots,p \tag{A8}$$

and thus $\vartheta(P(x,y)) = \arg[P(x,y)]$ gives induced average OP preference at (x,y).

This process reflects the influence of all completed local maps upon the surrounding field, and the calculations were iterated at each time step, with new local maps added in accord with the procedure next described.

C.2. Late phase: Placement of completed maps

At the subsequent time-step, values were then ascribed to a single further color wheel within an hexagonal element adjacent to one of the "seeding" maps. These newly ascribed values were those required to optimize the positioning of the new map in relation to its neighbors, minimizing the maximum angular disparity between the new map and the mirror-image of all its neighbors. Magnitude of the vector for the new map was set to unity. This process reproduces the settling into final stable states of adjacent local maps.

C.3. Temporal smoothing

The two phasic processes were each iterated at each time-step until the evolution of the field was complete. Temporal smoothing of successive time-steps then merged the early effects produced by existing local maps, with the final consolidated positions of new maps, into a continuous growth process.

Temporal smoothing was given by

$$P(x,y,t) = \sum_\tau P(x,y,t,\tau)/(1+|\tau|)^n, \quad \tau = -(t-t_0),\ldots,0,\ldots,(t_{\text{final}} - t), \tag{A9}$$

where τ is lag from the present time-step, t, and n is again a parameter varied from 1 to 3 in successive simulations to check that sensitivity of convergence to the final state was low.

Appendix D. Effect of velocity on orientation preference

Figs. 3 and 8 are schematic representations showing how the image of a moving object projected by the direct visual pathway to global V1, becomes relayed to a local map. Geometric relations arising from Fig. 8 are:

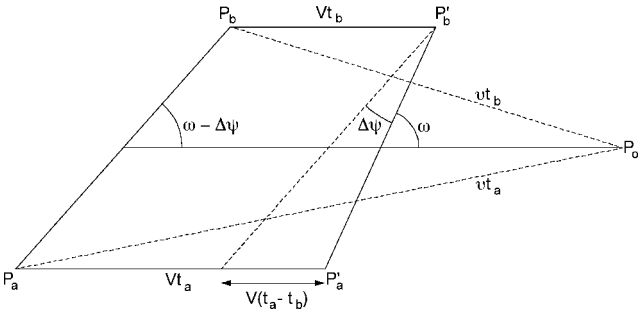

If O^+ is traveling at a velocity $\mathbf{v}$ at angle ω with respect to $P'_aP'_b$ and angle ψ with respect to the reference frame of $\{P\}$, then

$$P'_b = P_b + \mathbf{v}t_b \text{ and } P'_a = P_a + \mathbf{v}t_a, \text{ where}$$

$$t_a = \left|\frac{P_a - P_0}{\upsilon}\right| \text{and } t_b = \left|\frac{P_b - P_0}{\upsilon}\right|, \tag{A10}$$

$P_aP'_a$ and $P_bP'_b$ are parallel to the direction of $\mathbf{v}$, since they are loci of the movement of O^+. Utilizing a constructed line through P'_b, parallel to P_aP_b, by use of properties of parallels and the sine rule $\frac{\sin\Delta\psi}{|\mathbf{v}t_a - \mathbf{v}t_b|} = \frac{\sin(\pi-\omega)}{|P_a - P_b|} = \frac{\sin(\omega-\Delta\psi)}{|P'_a - P'_b|}$, and thus

$$\Delta\psi = \sin^{-1}[\sin(\pi-\omega)\left|\frac{\mathbf{v}}{\upsilon}\right|(|P_a - P_0| - |P_b - P_0|)/|P_a - P_b|]. \tag{A11}$$

References

Alexander, D. M., Bourke, P. D., Sheridan, P., Konstandatos, O., & Wright, J. J. (1998). Emergent symmetry of local and global maps in the primary visual cortex: Self-organization of orientation preference. *Proceedings Complex Systems, 98*, 25–31.

Alexander, D. M., Bourke, P. D., Sheridan, P., Konstandatos, O., & Wright, J. J. (2004). Intrinsic connections in tree shrew V1 imply a global to local mapping. *Vision Research, 44*(9), 857–876.

Alexander, D.M., & Wright, J.J. (2006). The maximum range and timing of excitatory contextual modulation in monkey primary visual cortex. *Visual Neuroscience* (in press).

Angelucci, A., Levitt, J. B., Walton, E. J. S., Hupe, J-M., Bullier, J., & Lund, J. S. (2002). Circuits for local and global signal integration in primary visual cortex. *Journal of Neuroscience, 22*(19), 8633–8646.

Angelucci, A., & Bullier, J. (2003). Reaching beyond the classical receptive field of V1 neurons; horizontal or feedback axons?. *The Journal of Physiology (Paris) 97*(2-3), 141–154.

Artola, A., Brocher, S., & Singer, W. (1990). Different voltage-dependent thresholds for the induction of long-term depression and long-term potentiation in slices of the rat visual cortex. *Nature, 347*, 69–72.

Basole, A., White, L. E., & Fitzpatrick, D. (2003). Mapping of multiple features in the population response of visual cortex. *Nature, 423*, 986–990.

Bienenstock, E., Cooper, L. N., & Monro, P. W. (1982). Theory for the development of neuron selectivity: Orientation specificity and binocular interaction in visual cortex. *Journal of Neuroscience, 2*, 32–48.

Blakemore, C. (1976). Modification of visual function by early visual experience. *Bulletin der Schweizerischen Akadeie der Medizinischen Wissenschaften, 32*, 13–28.

Blakemore, C., Movshon, J. A., & Sluyters, R. C. (1978). Modification of the kitten's visual cortex by exposure to spatially periodic patterns. *Experimental Brain Research, 31*, 651–672.

Blasdel, G. G., & Lund, J. S. (1983). Termination of afferent axons in macaque striate cortex. *Journal of Neuroscience, 3*, 1389–1413.

Bosking, W. H., Zhang, Y., Schofield, B., & Fitzpatrick, D. (1997). Orientation selectivity and the arrangement of horizontal connections in tree shrew striate cortex. *Journal of Neuroscience, 17*(6), 2112–2127.

Braitenberg, V. (1978). Cortical architectonics: General and areal. In M. A. B. Brazier & H. Petsch (Eds.), *Architectonics of the cerebral cortex*. Raven Press.

Braitenberg, V., & Schuz, A. (1998). *Cortex: Statistics and geometry of neuronal connectivity*. Berlin: Springer-Verlag.

Bressloff, P. C., & Cowan, J. D. (2002). S(O3) symmetry breaking mechanism for orientation and spatial frequency tuning in visual cortex. *Physical Review Letters, 88*, 078102.

Bressloff, P. C. (2002). Bloch waves, periodic feature maps and cortical pattern formation. *Physical Review Letters, 89*, 088101.

Cavanaugh, J. R., Bair, W., & Movshon, J. A. (2002). Nature and interaction of signals from the receptive field center and surround in Macaque V1 neurons. *Journal of Neurophysiology, 88*(5), 2530–2546.

Chavane, F., Monier, C., Bringuier, V., Baudot, P., Borg-Graham, L., Lorenceau, J., et al. (2000). The visual cortical association field: A gestalt concept or a psychophysiological entity. *Journal of Physiology (Paris), 94*, 333–342.

Chapman, B., Stryker, M. P., & Bonhoeffer, T. (1996). Development of orientation preference maps in ferret primary visual cortex. *Journal of Neuroscience, 16*, 6443–6453.

Chapman, C. L., Bourke, P. D., & Wright, J. J. (2002). Spatial eigenmodes and synchronous oscillation: Coincidence detection in simulated cerebral cortex. *Journal of Mathematical Biology, 45*, 57–78.

De Valois, K. K., De Valois, R. L., & Yund, E. W. (1979). Responses of striate cortical cells to grating and checkerboard patterns. *Journal of Physiology, 291*, 483–505.

Das, A., & Gilbert, C. D. (1999). Topography of contextual modulations mediated by short-range interactions in primary visual cortex. *Nature, 399*, 655–661.

Durbin, R., & Willshaw, D. J. (1987). An analogue approach to the travelling salesman problem using an elastic net method. *Nature, 326*, 689–691.

Durbin, R., & Mitchison, G. (1990). A dimension reduction framework for understanding cortical maps. *Nature, 343*, 644–647.

Ernst, U. A., Pawelzik, K. R., Sahar-Pikielny, C., & Tsodyks, M. V. (2001). Intracortical origin of visual maps. *Nature Neuroscience, 4*(4), 431–436.

Fiorani, M., Jr., Rosa, M. G., Gattass, R., & Rocha-Miranda, C. E. (1992). Dynamic surrounds of receptive fields in primate striate cortex: A physiological basis for perceptual completion? *Proceeding of the National Academy of Sciences of the United States of America, 89*(18), 8547–8551.

Fitzpatrick, D., Lund, J. S., & Blasdel, G. G. (1985). Intrinsic connections of macaque striate cortex: Afferent and efferent connections of lamina 4C. *Journal of Neuroscience, 5*, 3329–3349.

Freeman, W. J. (1975). *Mass action in the nervous system*. New York: Academic Press.

Goodhill, G. J. (1993). Topography and ocular dominance: A model exploring positive correlations. *Biological Cybernetics, 69*, 109–118.

Gray, C. M., Konig, P., Engel, A. K., & Singer, W. (1989). Oscillatory responses in cat visual cortex exhibit intercolumnar synchronisation which reflects global stimulus properties. *Nature, 388*, 334–337.

Gray, C. M., Engel, A. K., Konig, P., & Singer, W. (1992). Synchronization of oscillatory neuronal responses in cat striate cortex: Temporal properties. *Visual Neuroscience, 8*, 337–347.

Grossberg, S., & Williamson, J. R. (2001). A neural model of how horizontal and interlaminar connections of visual cortex develop into adult circuits that carry out perceptual grouping and learning. *Cerebral Cortex, 11*, 37–58.

Haken, H. (1996). *Principles of brain functioning*. Heidelberg, Berlin, New York: Springer.

Hancock, P. J. B., Smith, L. S., & Phillips, W. A. (1991). A biologically supported error-correcting learning rule. *Neural Computation, 3*, 201–212.

Hubel, D. H., & Wiesel, T. N. (1968). Receptive fields and functional architecture of the monkey striate cortex. *Journal of Physiology, 195*, 215–243.

Hubel, D. H., & Wiesel, T. N. (1977). Functional architecture of macaque monkey visual cortex. *Proceedings of the Royal Society (B), 198*, 1–59.

Jirsa, V. K., & Haken, H. (1996). Field theory of electromagnetic brain activity. *Physical Review Letters, 77*, 960–963.

Kandel, E. R., & Schwartz, J. H. (1985). *Principles of neural science* (2 ed.). New York, Amsterdam, Oxford: Elsevier, pp. 757–770..

Kang, K., Shelley, M., & Sompolinsky, H. (2003). Mexican hats and pinwheels in visual cortex. *Proceeding of the National Academy of Sciences of the United States of America, 100*, 2848–2853.

Kay, J., & Phillips, W. A. (1997). Activation functions, computational goals and learning rules for local processors with contextual guidance. *Neural Computation, 9*, 763–778.

Kirkpatrick, S., Gelatt, C. D., & Vecchi, M. P. (1983). Optimization by simulated annealing. *Science, 220*, 671–680.

Kohonen, T. (1982). Self-organized formation of topologically correct feature maps. *Biological Cybernetics, 43*, 59–69.

Lamme, V. A. F., Super, H., & Spekreijse, H. (1998). Feedforward, horizontal and feedback processing in the visual cortex. *Current Opinion in Neurobiology, 8*, 529–535.

Lee, T. S. (2002). Top-down influence on early visual processing: A Bayesian perspective. *Physiology & Behavior, 77*, 645–650.

LeVay, S., Wiesel, T. N., & Hubel, D. (1981). The post-natal development and plasticity of ocular-dominance columns in the monkey. In F. O. Schmitt, F. G. Worden, G. Adelman, & S. G. Dennis (Eds.), *The organization of the cerebral cortex* (pp. 29–45). Cambridge, MA: MIT Press.

Levitt, J. B., & Lund, J. S. (2002). The spatial extent over which neurons in macaque striate cortex pool visual signals. *Visual Neuroscience, 19*(4), 439–452.

Li, W., Their, P., & Wehrhahn, C. (2000). Contextual influence on orientation discrimination of humans and responses of neurons in V1 of alert monkeys. *Journal of Neurophysiology, 83*(2), 941–954.

Liley, D. T. J., & Wright, J. J. (1994). Intracortical connectivity of pyramidal and stellate cells: Estimates of synaptic densities and coupling symmetry. *Network: Computation in Neural Systems, 5*, 175–189.

Linsker, R. (1986). From basic network principles to neural architecture: Emergence of orientation columns. *Proceedings of the National Academy of Sciences of the United States of America, 83*, 8779–8783.

Malach, R., Amir, Y., Harel, M., & Grinvald, A. (1993). Relationship between intrinsic connections and functional architecture revealed by optical imaging and in vivo targeted biocytin injections in primate striate cortex. *Proceedings of the National Academy of Sciences of the United States of America, 90*(22), 10469–104973.

Miller, K. D., Keller, J. B., & Stryker, M. P. (1989). Ocular dominance column development : Analysis and simulation. *Science, 245*, 605–615.

Mitchison, G., & Durbin, R. (1986). Optimal numberings of an $N \times N$ array. *SIAM Journal of Algebraic and Discrete Methods, 7*, 571–578.

Mountcastle, V. B. (1979). An organizing principle for cerebral function: The unit module and the distributed system. In F. O. Schmitt & F. G. Worden (Eds.), *The neurosciences 4th study program*. Cambridge, MA: MIT Press.

Movshon, J. A., Thompson, I. D., & Tolhurst, D. J. (1978). Receptive field organization of complex cells in the cat's striate cortex. *Journal of Physiology, 283*, 79–99.

Nunez, P. (1995). *Neocortical dynamics and human eeg rhythms*. New York, Oxford: Oxford University Press, pp. 109–123.

Obermayer, K., Ritter, H., & Schulten, K. (1990). A principle for the formation of the spatial structure of cortical feature maps. *Proceedings of the National Academy of Sciences of the United States of America, 87*, 8345–8349.

Obermayer, K., & Blasdel, G. G. (1993). Geometry of orientation and ocular dominance columns in monkey striate cortex. *Journal of Neuroscience, 13*(10), 4114–4129.

Peck, C. K., & Blakemore, C. (1975). Modification of single neurons in the kitten's visual cortex after brief periods of monocular visual experience. *Experimental Brain Research, 22*, 57–68.

Phillips, W. A., & Singer, W. (1997). In search of common foundations for cortical computation. *Behavioural and Brain Sciences, 20*, 657–722.

Rennie, C. J., Wright, J. J., & Robinson, P. A. (2000). Mechanisms of cortical electrical activity and emergence of gamma rhythm. *Journal of Theoretical Biology, 205*(1), 17–35.

Ringach, D. L., Hawken, M. J., & Shapley, R. (1997). Dynamics of orientation tuning in macaque primary visual cortex. *Nature, 387*, 281–284.

Robinson, P. A., Rennie, C. J., & Wright, J. J. (1998). Synchronous oscillations in the cerebral cortex. *Physical Review E, 57*, 4578–4588.

Robinson, P. A., Rennie, C. J., Rowe, D. L., O'Connor, S. C., Wright, J. J., Gordon, E., et al. (2003). Neurophysical modeling of brain dynamics. *Neuropsychopharmacology, 28*, S74–S79.

Rossi, A. F., Desimone, R., & Ungerleider, L. G. (2001). Contextual modulation in primary visual cortex of Macaques. *Journal of Neuroscience, 21*(5), 1698–1709.

Ruthazer, E. S., & Stryker, M. P. (1996). The role of activity in the development of long-range horizontal connections in area 17 of the ferret. *Journal of Neuroscience, 16*, 7253–7269.

Schiller, P. H., Finlay, B. L., & Volman, S. F. (1976). Quantitative studies of single-cell properties in monkey striate cortex. V. Multivariate statistical analyses and models. *Journal of Neurophysiology, 39*(6), 1362–1374.

Series, P., Georges, S., Lorenceau, J., & Fregnac, Y. (2002). Orientation dependent modulation of apparent speed: A model based on the dynamics of feed-forward and horizontal connectivity in V1 cortex. *Vision Research, 42*, 2781–2797.

Singer, W., & Gray, C. M. (1995). Visual feature integration and the temporal correlation hypothesis. *Annual Review of Neuroscience., 18*, 555–586.

Slovin, H., Arieli, A., Hildesheim, R., & Grinvald, A. (2002). Long-term voltage-sensitive dye imaging reveals cortical dynamics in behaving monkeys. *Journal of Neurophysiology, 88*, 3421–3438.

Stein, A., & Sarnthein, J. (2000). Different frequencies for different scales of cortical integration: From local gamma to long range alpha/theta synchronisation. *International Journal of Psychophysiology, 38*, 301–313.

Steriade, M., Timofeev, I., & Grenier, F. (2001). Natural waking and sleep states: A view from inside neocortical neurons. *Journal of Neurophysiology, 85*, 1969–1985.

Sugita, Y. (1999). Grouping of image fragments in primary visual cortex. *Nature, 401*(6750), 269–272.

Swindale, N. V., Shoham, D., Grinvald, A., Bonhoeffer, T., & Hubener, M. (2000). Visual cortical maps are optimised for uniform coverage. *Nature Neuroscience, 3*(8), 822–826.

Swindale, N. V., Grinvald, A., & Shmuel, A. (2003). The spatial pattern of response magnitude and selectivity for orientation and direction in cat visual cortex. *Cerebral Cortex, 13*, 225–238.

Tanaka, S. (1989). Theory of self-organization of cortical maps. In D. S. Touretzky (Ed.), *Advances in neural information processing systems I* (pp. 451–458). San Mateo: Morgan Kauffman.

von der Marlsburg, C. (1973). Self-organization of orientation selective cells in the striate cortex. *Kybernetic, 14*, 85–100.

Weliky, M., Bosking, W. H., & Fitzpatrick, D. (1996). A systematic map of direction preference in primary visual cortex. *Nature, 379*(6567), 725–728.

Wright, J. J. (1997). EEG simulation: Variation of spectral envelope, pulse synchrony and 40 Hz oscillation. *Biological Cybernetics, 76*, 181–184.

Wright, J. J., Bourke, P. D., & Chapman, C. L. (2000). Synchronous oscillation in the cerebral cortex and object coherence: Simulation of basic electrophysiological findings. *Biological Cybernetics, 83*, 341–353.

Wright, J. J., Rennie, C. J., Lees, G. J., Robinson, P. A., Bourke, P. D., Chapman, C. L., et al. (2003). Simulated electrocortical activity at microscopic, mesoscopic and global scales. *Journal of Neuropsychopharmacology, 28*, S80–S93.

Yoshioka, T., Blasdel, G. G., Levitt, J. B., & Lund, J. S. (1996). Relation between patterns of intrinsic lateral connectivity, ocular dominance, and cytochrome oxidase-reactive regions in macaque monkey striate cortex. *Cerebral Cortex, 6*(2), 297–310.